



Article

Equivalent Hydraulic Conductivity of Heterogeneous Aquifers Estimated by Multi-Frequency Oscillatory Pumping

Avinoam Rabinovich * and David Guy

School of Mechanical Engineering, Tel Aviv University, Tel Aviv 69978, Israel

* Correspondence: avinoamr@tauex.tau.ac.il

Abstract: Aquifers are a vital part of our water cycle and modeling groundwater flow is paramount for a number of environmental applications. Modeling requires the estimation of aquifer properties, which is mostly achieved by field pumping tests. Oscillatory pumping tests involve repeated pumping and injection of aquifer water, which generates a periodic head signal. We investigate the estimation of equivalent hydraulic conductivity (K_{eq}) in an oscillatory pumping test with a multi-frequency excitation. Synthetic head data are generated from numerical simulations of pumping in heterogeneous aquifers and an inverse method is applied to estimate K_{eq} . The method involves a Fast Fourier Transform (FFT) analysis for obtaining the spatial distribution of head amplitude and then matching the amplitudes using a semi-analytical solution of a homogeneous aquifer with conductivity K_{eq} . We investigate the dependence of K_{eq} on pumping frequency in view of the previous literature, which has found increasing values for higher frequencies. We did not find this increase in K_{eq} with frequency and minor variations which were observed appear to be a result of numerical error. The result implies that oscillatory pumping field tests can be used for K_{eq} estimation without any corrections for frequency dependence.



Citation: Rabinovich, A.; Guy, D. Equivalent Hydraulic Conductivity of Heterogeneous Aquifers Estimated by Multi-Frequency Oscillatory Pumping. *Sustainability* **2023**, *15*, 13124. <https://doi.org/10.3390/su151713124>

Academic Editors: Alexandre Giacobbo, Margarida Oliveira and Igor Dias

Received: 24 July 2023

Revised: 19 August 2023

Accepted: 28 August 2023

Published: 31 August 2023



Copyright: © 2023 by the authors. Licensee MDPI, Basel, Switzerland. This article is an open access article distributed under the terms and conditions of the Creative Commons Attribution (CC BY) license (<https://creativecommons.org/licenses/by/4.0/>).

1. Introduction

A pumping test is a common method for estimating hydraulic conductivity (K) of aquifers, required for modeling flow in various environmental applications such as groundwater management [1], contaminant transport [2], CO₂ storage in saline aquifers [3] and managed aquifer recharge [4]. Oscillatory pumping tests are a unique type of test in which water is injected and produced in a repeated sequence in order to generate a periodic pressure signal. The signals are measured at various observation wells surrounding the pumping well and by comparison to a homogeneous aquifer model, the equivalent conductivity (K_{eq}) representing a homogeneous aquifer with approximately the same pressure signals as that of the actual heterogeneous aquifer is estimated. These tests have been shown to be useful and feasible for estimating K_{eq} (see references below), having a number of advantages in comparison to conventional pumping tests. However, in heterogeneous aquifers there has been evidence that the estimated K_{eq} values will vary depending on the applied frequency of pumping. This is an interesting phenomenon which deserves further study and may need to be taken into account during implementation of the method. The current work presents a framework for estimating aquifer equivalent conductivity considering multi-frequency pumping tests and investigates the frequency dependence of K_{eq} .

There is a significant body of existing literature dealing with periodic or oscillatory pumping tests. Early works laid down the foundations of this method [5–7] and these were followed by theoretical models [8–11], laboratory experiments [12,13] and field

experiments [9,14–20]. The basic and most common type of field test analysis [9,14–16] involves matching the pressure measurements in observation wells surrounding the pumping well with a model of flow in a homogeneous aquifer and this allows for the estimation of the equivalent aquifer properties such as the hydraulic conductivity (K_{eq}) and specific storage ($S_{s,eq}$). More advanced field tests consist of a large number of pressure measurements and implement an analysis aiming to estimate the spatial distribution of the hydraulic properties in a stochastic inverse approach known as oscillatory hydraulic tomography (OHT) [18–21]. In this work, we focus on K_{eq} estimation, which is the most fundamental property estimated in pumping tests. Even considering an OHT field campaign, K_{eq} is expected to be estimated as a first step before attempting to characterize heterogeneity.

Theoretical models of periodic pumping tests have been developed in parallel to field experiments. The basic solution of one-dimensional flow from a sinusoidal periodic steady source pertaining to a fully penetrating well in a confined aquifer was derived a long time ago [8]. This solution was extended to a partially penetrating well leading to a three-dimensional axisymmetric solution [9]. An alternative derivation is obtained by using the method of images [10] and the solution is also extended to include a phreatic aquifer. A solution to heterogeneous aquifers subjected to periodic pumping was derived in a stochastic approach, considering K as a random space variable [22]. Numerical solutions were also implemented in various works to solve for heterogeneous aquifers [20,23,24].

Most of the previous work on oscillatory pumping considers a pure sinusoidal pressure signal induced by the pumping well. We refer to these tests as single-frequency tests. However, the method can be applied considering pumping with multiple frequencies and this has been shown to improve K estimation [13,25]. This can be carried out by repeating single-frequency tests or by a single test in which the pumping signal is a sum of a number of sinusoidal pressure excitations; we refer to the latter as multi-frequency tests. Multi-frequency oscillatory pumping tests have been investigated by numerical simulations considering synthetic aquifers [24,26,27], and in a recent publication, an approach for K_{eq} estimation for multi-frequency tests was presented [28]. However, the suggested method was applied to a homogeneous aquifer using synthetic data generated by an analytical solution, while this work advances the study of heterogeneous aquifers and therefore considers numerically generated synthetic data.

Previous single-frequency field tests have estimated K_{eq} for a number of different periods of pumping. It was observed that K_{eq} varies with frequency [14–16] and a number of different hypotheses were offered for this phenomenon. One possible explanation is related to the changing attenuation of the pressure signal from the source, implying that equivalent properties effectively average over different regions of the aquifer for changing periods [23]. A second possibility is that the changes are related to a unique characteristic of equivalent properties in oscillatory flow. This was investigated in a number of theoretical studies regarding effective conductivity in heterogeneous media near a boundary of oscillating pressure [29,30] and also in a recent study of oscillatory pumping from a well [22]. It was found that the effective conductivity increases with increasing frequency as a result of a mechanism of preferential flow in higher conductivity regions. Despite the above literature, it is still unclear what, if any, is the significance of K_{eq} frequency dependence, and whether this phenomenon should be accounted for by practitioners conducting periodic pumping tests.

In this work, we present a framework for calculating equivalent conductivity from multi-frequency pumping tests and characterize the frequency dependence of K_{eq} . The first goal is to show the feasibility of using a multi-frequency pumping test to estimate K_{eq} by implementing the procedure on synthetic data obtained from numerical simulations of pumping in heterogeneous aquifers with random three-dimensional lognormally distributed K . The second goal is to investigate differences in the obtained K_{eq} associated with varying frequency to shed some light on this matter, in view of previous findings. We also present results for the estimation of numerical errors in oscillatory pumping models. This information is expected to be useful for anyone employing numerical models, which are

widely used in the literature and by practitioners, for example, during implementation of OHT methods.

The paper is structured as follows. In Section 2 we present the groundwater problem and corresponding mathematical model. The inverse problem of identifying K from pressure measurements is also described. In Section 3, we detail the method implemented to obtain K_{eq} using data from multi-frequency pumping tests. Section 4 provides the details of the numerical model and Section 5 presents the results for a number of test cases. The results are discussed in Section 6 and the final section is a report of the summary and conclusions of this work.

2. Problem Statement

We consider a confined aquifer of finite thickness D and infinite dimensions in the horizontal direction, as illustrated in Figure 1. A vertical pumping well of radius R_w is located below the origin of the axes. The well is open to the aquifer only in a section of length L_w , located at a depth starting from $D_w - L_w$ and up to a depth D_w . Pumping and injection of water is conducted in an oscillatory manner with a time-varying flow rate of $Q(t)$. Several observation wells are scattered throughout the aquifer as depicted in Figure 1 and these wells are used to measure the hydraulic head at specific points, marked in red. The location and number of the observations has practically no effect on the system and it only serves as a means of measurement. It does, however, affect the interpretation of the aquifer properties, as the interpretation may change with more available measurement points.

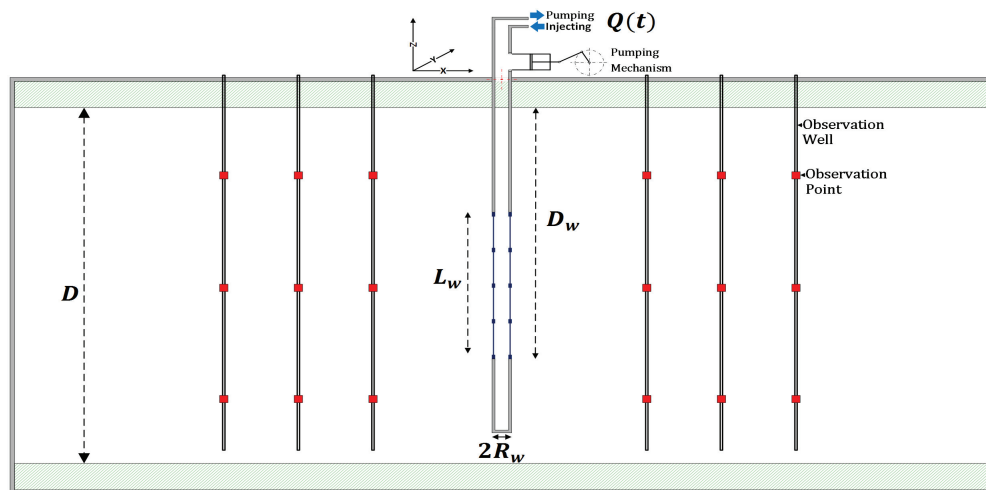


Figure 1. Setup of the pumping test problem.

The governing equation for this problem is given by

$$S(\mathbf{x}) \frac{\partial H(\mathbf{x}, t)}{\partial t} - \nabla [K(\mathbf{x}) \nabla H(\mathbf{x}, t)] = q_w(\mathbf{x}, t) \quad , \quad -D \leq z \leq 0 \quad (1)$$

where t (s) is time, H (m) is head, K (m/s) is conductivity, S (1/m) is specific storage, q_w (1/s) is the well term and $\mathbf{x} = (x, y, z)$ (m). Conductivity is taken to be a scalar function, i.e., we have assumed an isotropic K . The boundary conditions at the top and bottom of the impervious aquifer are given by

$$\frac{\partial H}{\partial z} = 0 \quad \text{at} \quad z = 0, \quad z = -D, \quad (2)$$

and far from the well, the boundary condition is given by

$$H \rightarrow 0, \quad R \rightarrow \infty, \quad (3)$$

where $R = (x^2 + y^2)^{1/2}$ is the horizontal coordinate. For single-frequency periodic pumping, the well discharge per length is a harmonic function of time, which can be expressed as the real part of a complex variable, i.e.,

$$Q_w(t) = |Q_w| \operatorname{Re} \left[\exp \left(\frac{2\pi i t}{P} \right) \right], \quad (4)$$

where $|Q_w|$ is the amplitude of the discharge per unit length, i is the imaginary unit number and P is the period of oscillations related to the angular frequency (ω) by $\omega = 2\pi/P$. Assuming that the well radius is sufficiently small ($R_w \ll D$), the well term in Equation (1) can be modeled as a line source and expressed as follows:

$$q_w(\mathbf{x}, t) = -|Q_w| \operatorname{Re} \left[\exp \left(\frac{2\pi i t}{P} \right) \right] [\chi(z + D_w) - \chi(z + L_w - D_w)] \delta(x) \delta(y), \quad (5)$$

where χ is the Heaviside step function and δ is the Dirac operator.

The governing equations can be reformulated using complex variables by considering a complex head $\tilde{H} = H \exp(-2\pi i t/P)$ and the complex well term given by Equation (5) (without taking the real part). Substituting these in Equation (1) leads to

$$\frac{2\pi i}{P} S \tilde{H} - K \nabla^2 \tilde{H} = -|Q_w| [\chi(z + D_w) - \chi(z + L_w - D_w)] \delta(x) \delta(y) \quad , \quad -D \leq z \leq 0 \quad (6)$$

and the boundary conditions are now

$$\frac{\partial \tilde{H}}{\partial z} = 0 \quad \text{at} \quad z = 0, \quad z = -D \quad (7a)$$

$$\tilde{H} \rightarrow 0 \quad , \quad R \rightarrow \infty. \quad (7b)$$

Solving this system of equations with complex variables and then taking the real part of the solution is equivalent to the original problem.

A solution to Equations (6) and (7) for the case of a homogeneous aquifer ($K = \text{const}$) was presented in the previous literature [10,16]. The exact semi-analytical solution for that case is given by

$$\tilde{H}^{hom}(R, z) = \frac{|Q_w|}{K} \int_{-D_w}^{-D_w + L_w} \left[\sum_{m=-\infty}^{\infty} \sum_{l=1}^2 G_{\infty} \left(R, z + (-1)^l z' + 2mD \right) \right] dz', \quad (8)$$

where the term G_{∞} is defined by

$$G_{\infty}(R, Z) = \exp \left[-\gamma \sqrt{R^2 + Z^2} \right] / (4\pi \sqrt{R^2 + Z^2}) \quad (9)$$

for any variable Z , and $\gamma = \sqrt{\pi S / (K P)}(i + 1)$. The number of terms taken in the infinite series in Equation (8) is determined by checking when convergence is achieved.

The mathematical problem described above is typically used for modeling periodic pumping tests despite simplifications which are considered in comparison to a real field pumping test, e.g., modeling the well as a line source or considering K as isotropic.

2.1. Multi-Frequency Problem

The problem presented previously can easily be restated considering a pumping source of multiple frequencies. In fact, even more generally, we can consider any well term expressed as a sum of N different terms, i.e.,

$$q_w(\mathbf{x}, t) = \sum_{n=1}^N q_{w,n}(\mathbf{x}, t). \quad (10)$$

Since the problem described by Equations (1)–(3) is linear, the solution is simply obtained by substituting each well term $q_{w,n}$ in Equation (1) and solving to obtain the head H_n . The final solution is the sum:

$$H(\mathbf{x}, t) = \sum_{n=1}^N H_n(\mathbf{x}, t). \quad (11)$$

In particular, any time-dependent pumping signal applied at a given well can be decomposed into a Fourier series and then the equations can be solved separately for each term in the series, thereby the solution is given by Equation (11). In this work, we will consider a multi-frequency pumping signal of the form

$$Q_{w,n}(t) = |Q_{w,n}| \operatorname{Re} \left[\exp \left(\frac{2\pi i t}{P_n} \right) \right], \quad (12)$$

where $|Q_{w,n}|$ is the amplitude of the n 'th term pertaining to frequency $\omega_n = 2\pi/P_n$ with a period P_n .

2.2. Nondimensionalization

We now normalize the parameters by a length scale $|Q_w|/K_{ref}$ and time scale $|Q_w|/K_{ref}^2$ (Q_w is discharge per unit length), where K_{ref} is some reference conductivity. The dimensionless parameters of the problem, denoted with an overline, are therefore taken to be $\overline{H} = \tilde{H}(\mathbf{x})K_{ref}/|Q_w|$, $\overline{K} = K(\mathbf{x})/K_{ref}$ and $\overline{\omega} = \omega S|Q_w|^2/K_{ref}^2$. It can be seen that the frequency ω and specific storage S are lumped together to form the dimensionless frequency. This is due to the fact that the two appear together in the homogeneous solution (see Equations (8) and (9)) and S will be considered a constant even when K is spatially varying (see Section 3). The spatial parameters will be normalized by the depth of the aquifer, i.e., $\overline{\mathbf{x}} = \mathbf{x}/D$, $\overline{D_w} = D_w/D$, $\overline{R} = R/D$ and $\overline{L_w} = L_w/D$.

2.3. Equivalent Conductivity Estimation

The problem of interest in this work is the calculation of equivalent hydraulic conductivity. An equivalent property of the aquifer pertaining to a certain point in space can be generally defined as that of a homogeneous medium, under the same boundary conditions and source term, which leads to approximately the same head response $H(t)$ as the one prevailing in the heterogeneous medium. Therefore, given a set of M head measurements $H_m(t)$ ($1 < m < M$) at various locations (m) in the heterogeneous aquifer, we are interested in finding a homogeneous aquifer with a hydraulic conductivity of K_{eq} such that it will have the closest possible head function $H_m^{hom}(t)$ to the measured $H_m(t)$ at all M locations. We note that while this approach has been adopted in the past (e.g., [16]) it is also common to calculate equivalent properties for each measurement point separately (e.g., [31]). For the purpose of investigating the frequency dependence of K_{eq} , it is more instructive to fit all measurements simultaneously to a single homogeneous model; however, we expect the conclusions of this work to remain the same for the second approach.

The approach for K_{eq} calculation described above can be applied for the time-dependent head signal $H_m(t)$ at all measurement locations m , considering a single-frequency periodic pumping flow rate. However, this requires matching a time data series at many locations. A more efficient approach is to carry out a Fourier analysis and decompose the periodic signal to simply an amplitude and phase shift at every measurement location. Therefore, the inverse problem requires only matching the two values (amplitude and phase) at each measurement point instead of a time series [16]. If the pumping signal contains multiple frequencies, K_{eq} can be calculated by matching the amplitude and phase at every measurement location and for all frequencies simultaneously. However, we are interested in investigating the frequency dependence of K_{eq} and therefore it will be calculated separately for each frequency. The full procedure is explained in the next section.

3. Method

We assume that M head time signals $H_m(t)$ have been measured at different spatial locations (m) in the domain. We further assume that the pumping rate is periodic with multiple frequencies and given by Equation (12), and that all the aquifer parameters (D , L_w , D_w) are known (see Figure 1). For simplicity, we also consider specific storage in the domain to be constant and known. Although this simplification is taken to enhance the accuracy of our results as we focus on the frequency dependence of K_{eq} , it is also a realistic assumption in many cases, as S tends to vary much less than K in heterogeneous aquifers (Section 3.2.1 in [32]). Furthermore, since we assume that S is constant and known, we do not require the phase shift in the inverse method and only amplitude is used. This also facilitates the investigation of the frequency dependence of K_{eq} . The procedure for calculating K_{eq} is as follows.

First, a Discrete Fourier Transform (DFT) is applied to each time data set of head $H_m(t)$. This results in an amplitude for each head measurement point m and for each frequency ω_n . We note that if the head data contain a transient part, measured before the system reaches a periodic steady state, then this part is removed from the data prior to the application of the DFT. Figure 2 illustrates this procedure, showing an example of a periodic head time function (Figure 2a) comprised of three sinusoidal functions with different frequencies and amplitudes (Figure 2b). The original signal is decomposed into the three source signals using a Fast Fourier Transform (FFT), which is an efficient algorithm for calculating the DFT of a data set [33]. The results of the FFT showing the amplitude in the frequency domain are presented in Figure 2c, where three distinct peaks are seen at $f = \omega / (2\pi) = 0.25, 0.5, 0.75$ (Hz), corresponding to the three frequencies of the source signals.

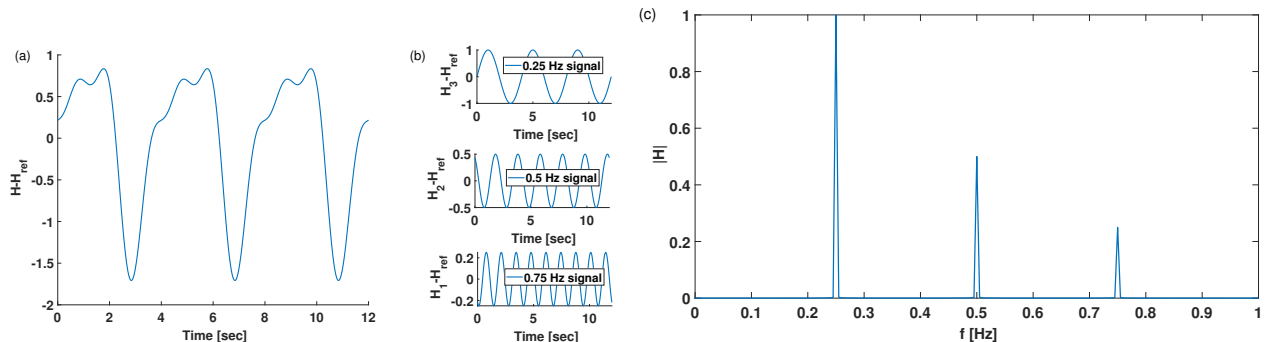


Figure 2. Example of head data processing (first step in method of Section 3). The measured head signal (a) is decomposed into the three sinusoidal signals (b) according to the FFT results (c).

The next step is to find the best fit of the homogeneous solution to the head data. We use the homogeneous solution given by Equations (8) and (9) with the known aquifer parameters and induced pumping frequencies. Varying K values are taken until the best match of the amplitude $|H_m^{hom}|$ with the measured data amplitudes $|H_m|$ at all locations m is found. Notice that the amplitude of the head time series is the same as the modulus of the complex head, i.e., $|H_m^{hom}(t)| = |\tilde{H}_m^{hom}|$. The problem of finding the best fit is described by the minimization of an objective function given by

$$Fit(K) = \sum_{m=1}^M \frac{|H_m| - |H_m^{hom}|}{|H_m^{hom}|}, \quad (13)$$

where H_m^{hom} of Equation (8) is a function of K and therefore Fit is also. We seek the K value which leads to the smallest Fit in Equation (13) and this will be defined as K_{eq} . As discussed in Section 2.1, the head solution for multi-frequency pumping can be calculated separately for each frequency and therefore the minimization procedure described above is repeated for each frequency separately so that K_{eq} is obtained for each frequency, i.e., we ultimately obtain $K_{eq}(\omega)$.

4. Numerical Experiments

We use synthetic data generated by a numerical simulator to represent the field data obtained in a pumping test. The problem presented in Section 2 is solved using the Groundwater Modeling System (GMS) simulation software (<https://www2.et.byu.edu/software/gms/gms.html>) [34], a commercial graphical user interface that utilizes the U.S. Geological Survey finite difference solver MODFLOW [35]. A three-dimensional model is constructed consisting of a square domain with $301 \times 301 \times 21$ cubic elements (in the x , y and z directions, respectively). The physical dimensions corresponding to the elements are $80 \times 80 \times 80$ m. The reason for the coarser element division in the z direction is the that we anticipate less variations in that direction than in the horizontal direction due to the nature of the line source. Although the line source is not fully penetrating, the vertical changes are expected to be less significant.

The boundary conditions at the top and bottom planes are set to be impermeable, i.e., no vertical flow, presented in Figure 3 by the blue highlighted elements and representing confined aquifer layers. The boundary condition for the infinite domain in the horizontal direction requires head values to approach zero as we approach infinity. However, since the model is finite, this condition is approximated by taking the four vertical faces of the domain to have zero head values, indicated by the orange dots in Figure 3. The applicability of this condition will be verified against the theoretical model in the next section (see Section 4.1).

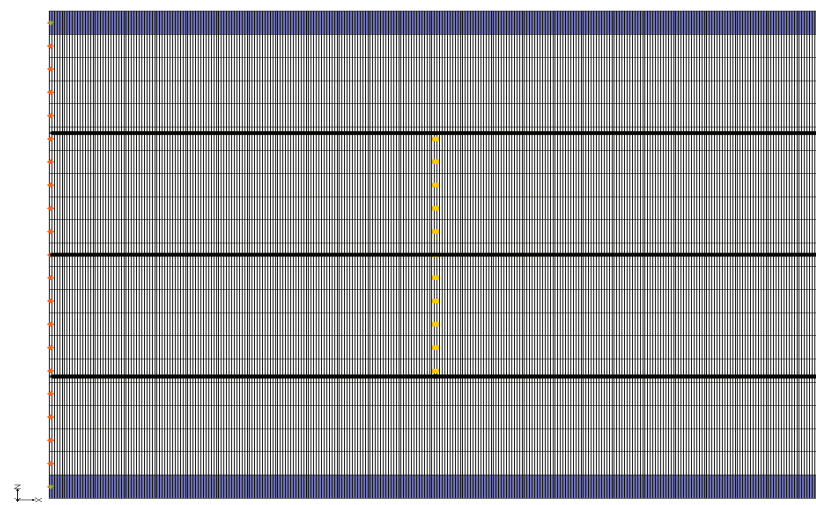


Figure 3. Cross section of the numerical model (located at the middle of the aquifer). Yellow points indicate the well and orange points represent a zero head boundary condition.

The discharge source is defined at the center of the domain, modeling a partially penetrating well, and spreads over several vertical elements at the center of the aquifer (yellow dots in Figure 3). The horizontal width of the well is one element, which is relatively small compared to the aquifer's horizontal extent, and can therefore be modeled by a line source in the equations (see Equation (5)). The flow rate of each source element is defined individually; however, they are all defined to be equal in order to simulate a uniform line source. To further ensure uniform pumping and injection, conductivity is defined to be a constant value for all well elements and taken to be $K = 3 \times 10^{-4}$ m/s or $K = 9.7 \times 10^{-5}$ m/s (for Case 1 and Case 2, respectively, as described in Section 5). Furthermore, in order to construct the multi-frequency signal accurately, the flow rate $Q_w(t)$ at each well element was set to be periodic with a small time step in the discrete representation of the $Q_w(t)$ function, so that it is much smaller than the smallest period, i.e., by at least an order of magnitude.

4.1. Validation and Error of Numerical Model

We now compare the numerical solution described above for the case of a homogeneous aquifer to the semi-analytical solution given by Equations (8) and (9). This is repeated for many parameters and the difference between the two solutions (i.e., the error) is quantified. There are two main reasons for the comparison. The first is to validate our numerical model, ensuring that the simulation performs in correspondence with the theoretical solution. The second is to map the errors between the theoretical and numerical solutions for a homogeneous aquifer, so that the errors can be used in the next section to indicate which numerical results are reliable for the heterogeneous aquifer solution.

We set the semi-analytical and numerical models to have the same aquifer depth of $D = 80$ m and as discussed previously, the horizontal dimensions of the numerical model are also 80 m. Conductivity is constant with a value of $K = 9.7 \times 10^{-5}$ m/s (equivalent to about 10 Darcy permeability) and the frequency of oscillations is chosen to be 0.1 Hz ($P = 62.8$ s). The other parameters are prescribed as $L_w = 40$ m, $D_w = 60$ m and $S = 1.5 \times 10^{-6}$ 1/m. Therefore, the dimensionless parameters of the problem are: $\bar{\omega} = 618$, $\bar{L}_w = 0.5$ and $\bar{D}_w = 0.75$, where we have taken the reference value $K_{ref} = 1.6 \times 10^{-4}$ m/s to be consistent with the value of steady state effective conductivity discussed in the next section.

Results for the semi-analytical and numerical solutions to the homogeneous aquifer problem at 3 different depths \bar{z} for the above parameters are presented in Figure 4. We note that \bar{z} is negative as the positive z direction is upward (see Figure 1). The amplitude solution is seen to decay exponentially with horizontal distance from the well, as expected by the known solution of the Green's function, i.e., G_∞ given by Equation (9). Furthermore, it can be seen that at all three depths, the semi-analytical and numerical solutions are in excellent agreement, therefore validating the numerical model. Nevertheless, we calculate the error of the numerical model simply by the absolute normalized difference, as follows:

$$Error = \left| \frac{|H_{analytical}| - |H_{numerical}|}{|H_{analytical}|} \right|. \quad (14)$$

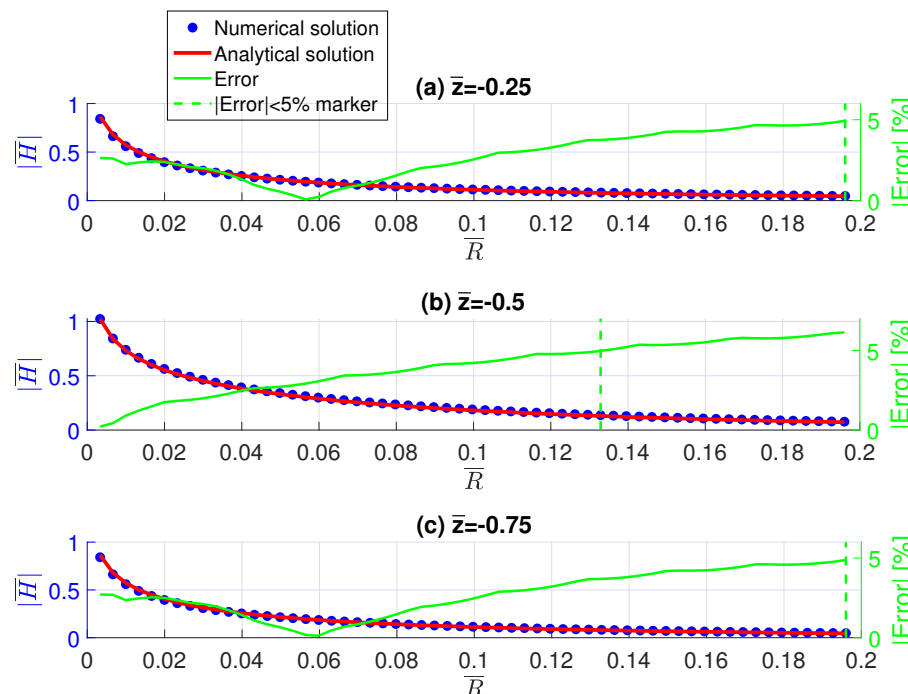


Figure 4. Comparison between the semi-analytical and numerical solutions for a homogeneous aquifer. Plotted is head amplitude as a function of horizontal distance from the well at three different depths and the error given by Equation (14).

The error is plotted in Figure 4 with a green curve, corresponding to the right y axis. It can be seen that errors are generally small, but increase with distance \bar{R} from the well. This increase is attributed to the small amplitude values far from the well which tend to generate more error as a result of the normalization.

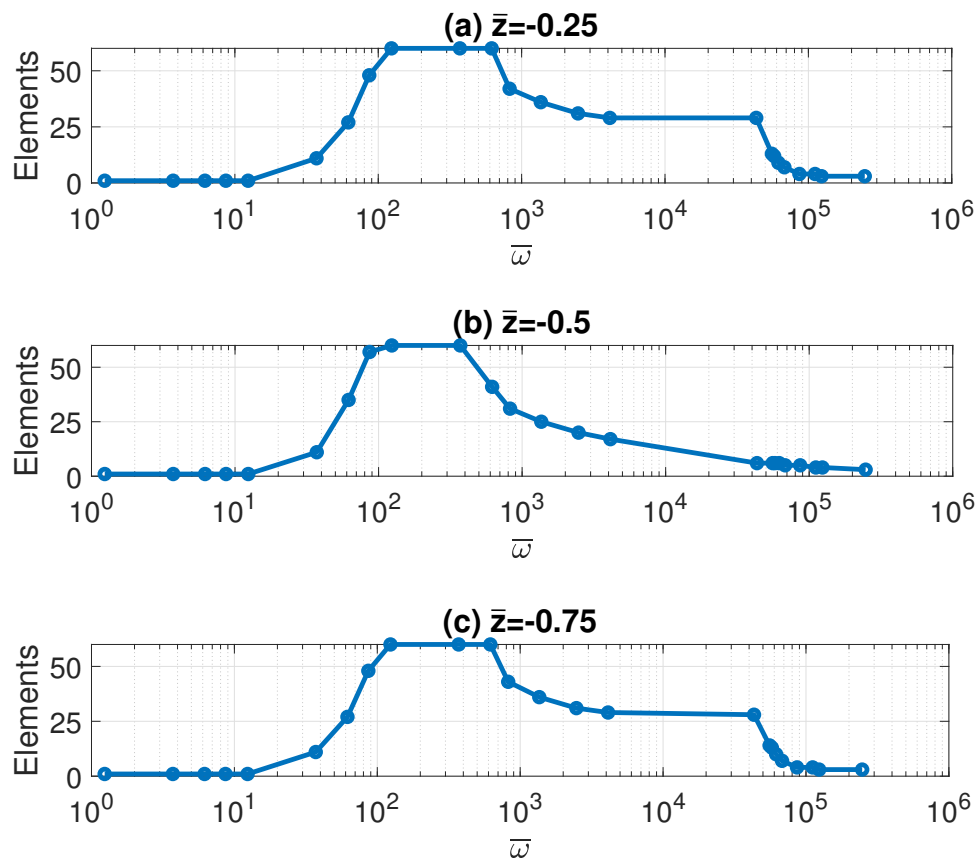
To avoid using erroneous measured head time signals H_m in the inverse method discussed in Section 3, we continue the error analysis. In this work, H_m is generated as synthetic data and therefore numerical errors in heterogeneous aquifer simulations will impact the accuracy of the K_{eq} estimations. We use the homogeneous aquifer error discussed above as an indication for the error that is likely to exist for the heterogeneous case. Therefore, we will only use data points which are in a certain region near the well, determined by a threshold of 5% error in Equation (14). As the error generally increases with distance, the 5% error criteria will result in a maximum distance from the well in which the head data can be used. This distance is indicated in Figure 4 with a green dashed line. This distance is also presented in Table 1 and Figure 5 for varying dimensionless frequencies. The distance is given in terms of the number of elements from the well with $Error < 5\%$. It can be seen that a wide range of frequencies spanning 5 orders of magnitude is tested and the distance varies significantly. For a large dimensionless frequency, the head attenuates rapidly with distance and therefore the numerical solution becomes inaccurate at a distance of only a few elements from the well. For a small dimensionless frequency, the head attenuates very slowly from the well so that it remains large at the boundaries (i.e., $\bar{R} = 1$), and therefore the boundary condition of $\bar{H} = 0$ applied to the numerical solution is no longer accurate and results in an error. It can be seen that for $\bar{\omega} < 12.4$ there is only a single block with smaller than 5% error, i.e., these cases cannot be used. Only for a range of intermediate values of $37.1 < \bar{\omega} < 6.18 \times 10^4$ there are sufficient elements to carry out the estimation of K_{eq} . We note that even in a real field test, the data which can be used for K_{eq} estimation will be limited by a maximum distance due to measurement errors associated with very small head amplitude; however, for low frequencies, there may not be a similar error (depending on the horizontal extent of the aquifer).

Table 1. A summary of simulations conducted for the homogeneous aquifer case and the number of elements from the well where $Error < 5\%$ for each depth and overall for all three depths.

$\bar{\omega}$	ω (Hz)	S (1/m)	$\bar{z} = -0.25$	$\bar{z} = -0.5$	$\bar{z} = -0.75$	Min	Overall
1.24	0.1	3×10^{-9}	1	1	1	1	1
3.71	0.1	9×10^{-9}	1	1	1	1	1
6.18	0.1	1.5×10^{-8}	1	1	1	1	1
8.66	0.1	2.1×10^{-8}	1	1	1	1	1
1.24×10^1	0.1	3×10^{-8}	1	1	1	1	1
3.71×10^1	0.1	9×10^{-8}	11	11	11	11	11
6.18×10^1	0.1	1.5×10^{-7}	27	35	27	27	27
8.66×10^1	0.1	2.1×10^{-7}	48	57	48	48	48
1.24×10^2	0.1	3×10^{-7}	60	60	60	60	60
3.71×10^2	0.1	9×10^{-7}	60	60	60	60	60
6.18×10^2	0.1	1.5×10^{-6}	60	41	60	41	41
8.24×10^2	0.1	2×10^{-6}	43	31	42	31	31
1.36×10^3	0.1	3.3×10^{-6}	36	25	36	25	25

Table 1. Cont.

$\bar{\omega}$	ω (Hz)	S (1/m)	$\bar{z} = -0.25$	$\bar{z} = -0.5$	$\bar{z} = -0.75$	Min Overall
2.47×10^3	0.1	6×10^{-6}	31	20	31	20
4.12×10^3	0.1	1×10^{-5}	29	17	29	17
4.33×10^4	0.1	1.05×10^{-4}	28	6	29	6
5.56×10^4	0.1	1.35×10^{-4}	14	6	13	6
5.77×10^4	0.1	1.4×10^{-4}	13	6	12	6
6.18×10^4	0.1	1.5×10^{-4}	10	6	9	6
6.8×10^4	0.1	1.65×10^{-4}	7	5	7	5
8.66×10^4	0.1	2.1×10^{-3}	4	5	4	5
1.11×10^5	0.1	2.7×10^{-3}	4	4	4	4
1.24×10^5	0.1	3×10^{-3}	3	4	4	4
2.47×10^5	0.1	6×10^{-3}	3	3	4	3

**Figure 5.** Number of elements extending radially from well with *Error* < 5% (see Equation (14)) at three different depths.

Two additional validations are conducted. The first is a validation of the linearity of the numerical model. The numerical solution is generated for a multi-frequency signal and using an FFT analysis, the head amplitude with distance from the well is obtained for each frequency. Then, the problem is solved for each frequency separately and the head amplitude is compared to the multi-frequency calculation showing excellent agreement. The second validation entails implementing the method of Section 3 on data generated by a homogeneous aquifer model. Since we are using the homogeneous theoretical solution

in the inverse algorithm, we should obtain that K_{eq} is equal to the simulation's constant K value, regardless of the problem parameters such as frequency or the specific storage. Indeed, this was verified and gave us the confidence to move forward with estimating K_{eq} for heterogeneous cases.

4.2. Conductivity Model

To model the aquifer hydraulic conductivity, we generate random three-dimensional fields of lognormally distributed values using the Stanford Geostatistical Modeling Software (SGeMS) (<http://sgems.sourceforge.net/>) [36] with the Sequential Gaussian Simulation [37] package. This is a typical structure used in the literature to model heterogeneous aquifers [32,38,39]. The conductivity is generated with a geometric mean of $K_G = 9.7 \times 10^{-5}$ m/s (equivalent to a permeability of 10 Darcy), log-variance of $\sigma_Y^2 = 4$ ($Y = \ln K$), and two cases of different correlation lengths: Case 1 consists of a dimensionless correlation of $l = 0.01$ (normalized by the domain length) and Case 2 is taken with $l = 0.06$. The conductivity realizations used in this work are plotted in Figure 6, presented as two cross sections through the center of the domain. It can be seen that in the x - y planes (Figure 6a,c), conductivity appears to be statistically isotropic while in the x - z planes (Figure 6b,d), the conductivity is anisotropic with elongated structures in the vertical direction. This is a result of the significantly smaller number of elements in the vertical direction (21) in comparison to the horizontal (301). Furthermore, the conductivity in Case 1 is seen to have a smaller correlation length than in Case 2, as prescribed. For reference, we calculate the steady state effective conductivity assuming isotropic K by the theoretical approximate relationship [40]:

$$K_{ef}^{st} = K_G(1 + \sigma_y^2/6) \quad (15)$$

and arrive at the value of $K_{ef}^{st} = 1.6 \times 10^{-4}$ m/s.

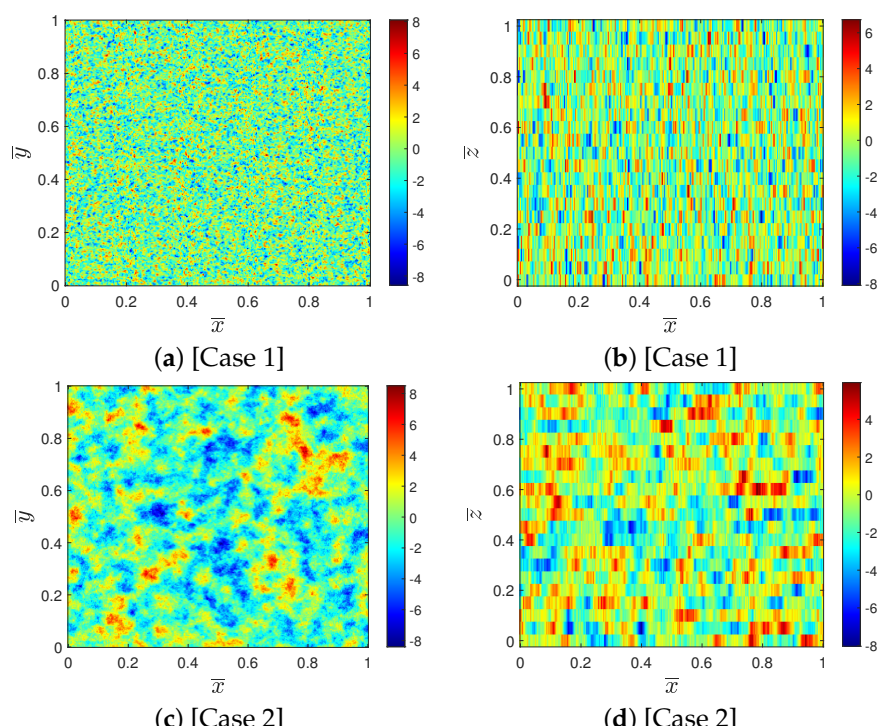


Figure 6. Spatial distribution of log-conductivity used as input for generating synthetic head data via numerical simulations for the two cases discussed in the text. Vertical and horizontal cross sections (\bar{x} is the primary flow direction) are presented through the center of the domain.

5. Results

The synthetic data are generated by conducting simulations as described in Section 4 with the parameters detailed therein. The specific storage is varied between the different simulations and the source is taken to consist of multiple frequencies. The method detailed in Section 3 is applied to the head data from the simulations and this leads to an estimation of \bar{K}_{eq} for each frequency $\bar{\omega}$. The results for Case 1 are plotted in Figure 7, where each set of connected data points represent data from a single multi-frequency simulation with a given S , as presented in the legend. It can be seen that the results are consistent for changing S and ω with the same $\bar{\omega}$ value, i.e., \bar{K}_{eq} is roughly the same for different numerical experiments with the same $\bar{\omega}$. Furthermore, in the range of $2 \times 10^5 < \bar{\omega} < 10^9$, equivalent conductivity is roughly constant at $\bar{K}_{eq} \simeq 0.43$ corresponding to the steady state value.

The steady state equivalent conductivity plotted in Figure 7 is calculated by carrying out a separate simulation of uniform mean flow and substituting the pressure drop in Darcy's law. The obtained dimensionless value is 0.43 which is about half of the steady state effective conductivity K_{eq}^{st} calculated by Equation (15) and used as a reference value in our nondimensionalization. The difference is due to the anisotropy of K in Case 1 (see Figure 6b), which is seen to have vertically elongated structures leading to $K_{eq} < K_{eq}^{st}$ (at the limit of layered K perpendicular to the imposed flow, the effective conductivity is the harmonic average, which is the lower bound).

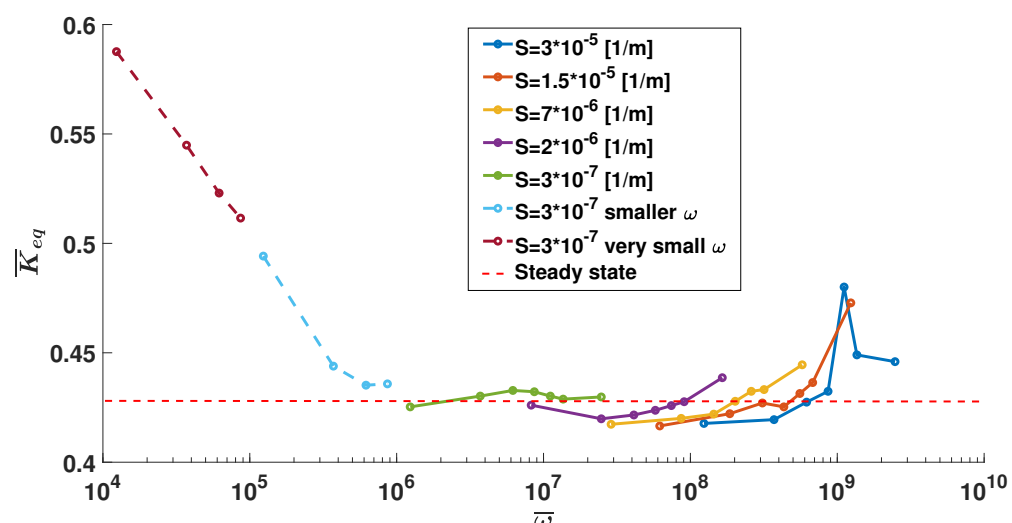


Figure 7. Dimensionless equivalent conductivity as a function of dimensionless frequency for Case 1 with varying specific storage and frequency of oscillations. The steady state value is presented for comparison.

For the large and small values of $\bar{\omega}$ in Figure 7, an increase in \bar{K}_{eq} is observed. This appears to be a result of numerical errors, as we have already observed in Section 4.1 that they increase for large and small values of $\bar{\omega}$ (see Figure 5). To illustrate this, we plot the error of the homogeneous simulations given by Equation (14) as a function of $\bar{\omega}$ in Figure 8. We note that the values of $\bar{\omega}$ in the bottom axis of the figure correspond to those in Figure 7 but not to those in Figure 5 (the nondimensionalization is different due to a larger injection amplitude). The green curve represents the error averaged over the five elements closest to the well in the two horizontal directions and for three depths: $\bar{z} = -0.25, -0.5$ and -0.75 . These are exactly the elements that were taken for the calculation of K_{eq} in Figure 7. It can be seen that a sharp increase in error occurs at around $\bar{\omega} = 10^5$ and a smaller increase at around $\bar{\omega} = 10^9$, corresponding to an increase in \bar{K}_{eq} at these locations. The red curve presents the error averaged over only the cells which have an error smaller than 5%; their number is presented in Table 1. It can be seen that the error remains low as expected; however, the curve is missing in the low $\bar{\omega}$ range in which \bar{K}_{eq} increases simply because

there are no blocks with $Error < 5\%$ in this range. At the high $\bar{\omega}$ range, the error is lower when taking only the $Error < 5\%$ blocks, as these blocks are only few in number (fewer than 5) and near the well (see Table 1).

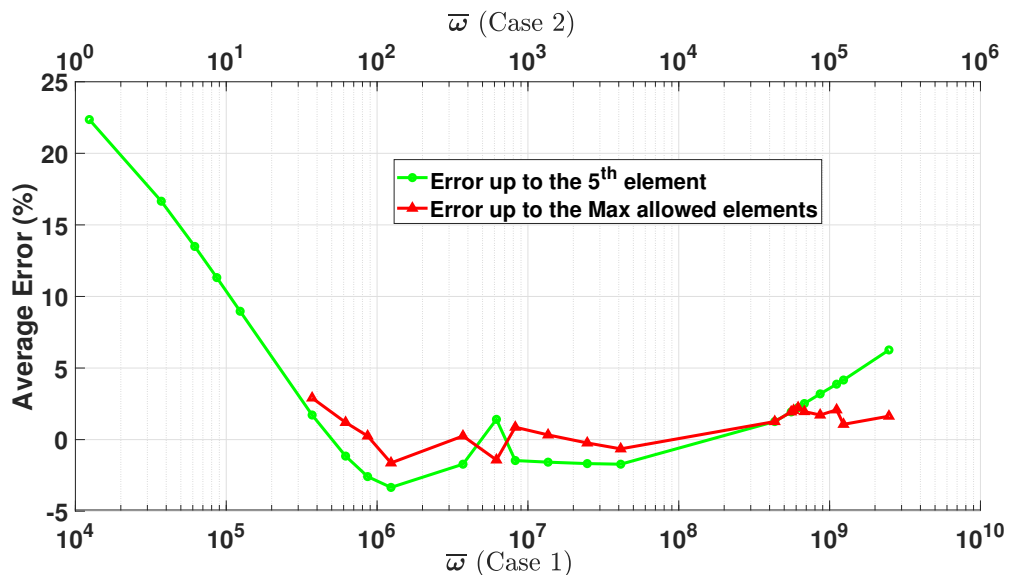


Figure 8. Error as calculated by Equation (14) averaged over all head data (H_m) as a function of dimensionless frequency.

We now wish to test whether the calculated equivalent conductivity captures the statistics of the entire domain and not only a small region near the well, as we only considered five elements near the well in our calculation. Taking five elements is not only necessary due to numerical errors, it is also realistic considering some field pumping tests, as the pressure signal attenuates leading to small head values which may be difficult to measure. In Figure 9, we plot the geometric and arithmetic averages of the conductivity field as a function of distance from the well, indicated by the element number in the x axis. It can be seen that for Case 1 (Figure 9a,b), the curve levels off rapidly with distance and the average values converge to a constant value. This behavior is due to the small correlation length. Therefore, after five elements, the averages are already approximately at the constant value representing the entire domain. This analysis helps to determine that for Case 1, the equivalent conductivity calculated using five elements indeed represents the entire domain. This is also supported by the fact that the \bar{K}_{eq} values are approximately the same as the steady state equivalent conductivity representing the entire domain (see Figure 7).

Figure 10 presents results for Case 2, which consists of a K distribution with a larger correlation length than in Case 1 (see Figure 6). The procedure for estimating K_{eq} described in Section 3 is applied to the synthetic head data; however, only single frequency simulations were carried out rather than multi-frequency ones conducted for Case 1. This is carried out in order to avoid possible errors associated with the FFT analysis. Furthermore, all locations which showed an error smaller than 5% in the evaluation conducted in Section 4.1 (see Table 1) were used in the analysis. Therefore, for each frequency, a different number of elements was used for K_{eq} calculation. The analysis was carried out for each depth ($\bar{z} = -0.25, -0.5$ and -0.75) separately as well as for all three depths together. It can be seen that for the overall analysis (combining the three depths), \bar{K}_{eq} remains fairly constant with changing $\bar{\omega}$. However, there is some variation apparent in the enlarged plot in Figure 10b, where a change of about 15% in \bar{K}_{eq} is observed. It can also be seen in the figure that the results of data only from the middle depth are similar to the overall results; however, the top and bottom depths present significant difference both in \bar{K}_{eq} values and in the variation with $\bar{\omega}$. The difference in the results of the depths could be a result of

changes in local heterogeneity or the impact of the top and bottom boundary conditions. Nevertheless, the agreement between the results for $\bar{z} = -0.5$ and those the combined three depths indicates robustness of the latter result, which will be considered the overall \bar{K}_{eq} for the domain.

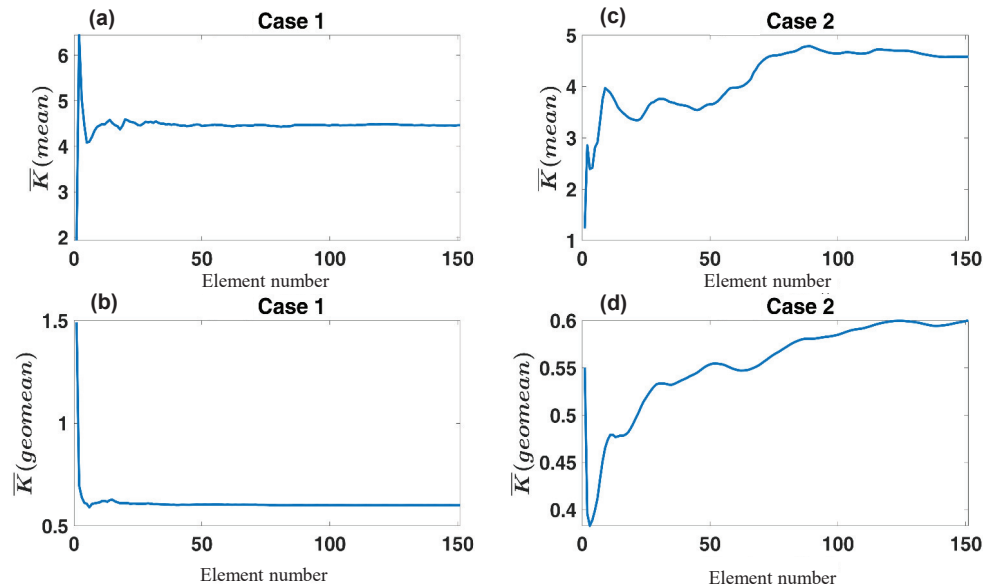


Figure 9. Average conductivity as a function of element number (representing the radial distance from the well). Both the arithmetic mean (a,c) and geometric mean (b,d) are plotted for each case.

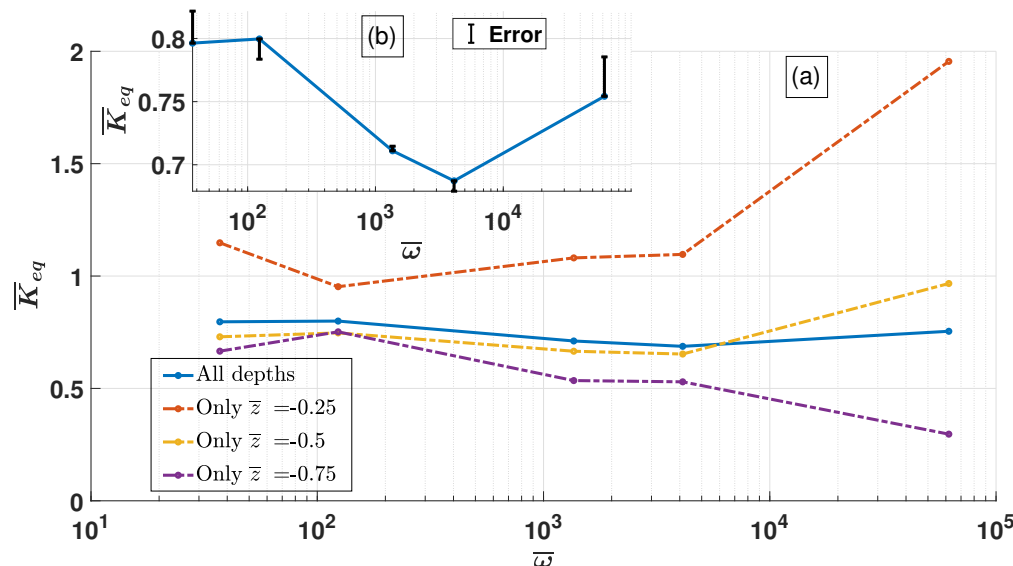


Figure 10. Dimensionless equivalent conductivity as a function of dimensionless frequency for Case 2. The inset (b) is an enlargement of the blue curve representing K_{eq} estimation using data from all depths.

The variation of the overall \bar{K}_{eq} can be considered minor; however, it is still more significant than in Case 1. This is seen clearly in Figure 11, where both cases are plotted together. The x-axis in the figure consists of dimensional values of $\omega \times S$ [$1/(m \times s)$] since the dimensionless $\bar{\omega}$ is not consistent between the two cases. \bar{K}_{eq} in Case 1 hardly varies, with a maximum change of 6%, as opposed to the 15% change seen in Case 2. The enhanced variations could be related to the different number of elements used in the analysis for each frequency, as the averages of the conductivity plotted in Figure 9c,d are seen to be somewhat varying in the range of elements used (6–60, see Table 1). To test this possibility,

we plot in Figure 11 the \bar{K}_{eq} calculation using only five elements closest to the well for all frequencies (same as in Case 1). It can be seen that the \bar{K}_{eq} values are slightly lower when using only five elements near the well and this is in agreement with the lower values for $\langle K \rangle$ observed in Figure 9c,d when averaging only over elements near the well (element number < 5). However, the trend of K_{eq} with increasing $\omega \times S$ is similar when using only five elements or with a changing number of elements and therefore it does not appear to explain the variations. We note that the overall values of Case 2 ($\bar{K}_{eq} \approx 0.75$) are larger than those of Case 1 ($\bar{K}_{eq} \approx 0.43$) since the steady state K_{eq} is also larger due to the larger correlation length.

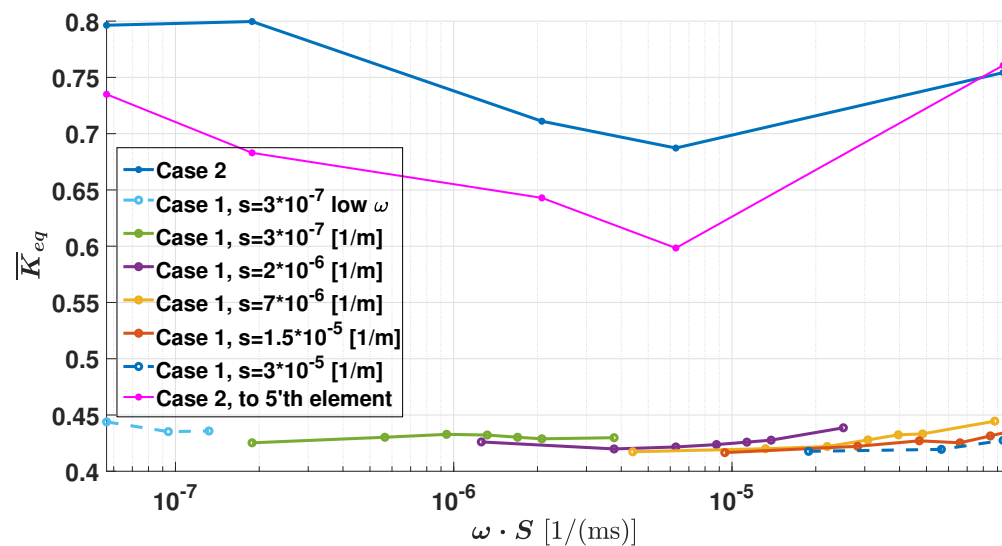


Figure 11. Dimensionless equivalent conductivity as a function of the product of frequency and specific storage for both cases.

In Figure 10b, we plotted error bars for the \bar{K}_{eq} results of Case 2. These are obtained by considering the error from the homogeneous case (presented in the red curve in Figure 8) and applying that error to the head values used in the estimation of \bar{K}_{eq} to obtain the error in terms of the equivalent property. While it can be seen that the errors are generally small (since we used only elements with head error less than 5%) it is apparent that the errors for the two middle points are much smaller than the other points. This could indicate that numerical errors are responsible for the variations seen in \bar{K}_{eq} values. It is reminded that the estimated errors are for the homogeneous case, while the data are generated for the heterogeneous case, which could have more significant errors.

6. Discussion

The results presented above advance the knowledge with respect to the previous literature in a number of ways. First, the framework for K_{eq} estimation given multi-frequency pumping data is different than in the previous literature. While a similar approach was described in the past [16], only a single frequency was considered there. Other publications [25,26] considered multi-frequency tests; however their purpose was to estimate K variation and not a single constant K_{eq} . Another work [28] presented a workflow which is different than the current one, as it includes optimization under uncertainty and assumes a homogeneous aquifer in the synthetic data testing. The second advancement of this work is the application of the presented workflow to synthetic head data from a periodic pumping test in a random heterogeneous aquifer, which has not been previously conducted. Third and most importantly, the frequency dependence was studied here in detail to advance our understanding of frequency-dependent equivalent conductivity. We found no significant change of K_{eq} with frequency, despite a large range of parameters that were tested and two cases of heterogeneous aquifer models.

To further discuss the variation of K_{eq} with frequency, we turn to the previous literature in which the variations were shown to be a result of a physical phenomenon. These were the motivation for this study. For an oscillating pressure boundary, previous work [30] plotted the dimensionless effective conductivity as a function of dimensionless frequency given by $\omega Sl/K_G$. Considering the properties of Case 2, the dimensionless frequency is between 0.05 and 8.4, which according to their analysis (see Figure 2 in [29]) should lead to a significant increase in \bar{K}_{eq} with frequency. However, we observe in our results a decrease of about 15%, followed by an increase of similar size. Our results are not in agreement with these and other [16,29] theoretical results and this is most likely due to the different conditions: (1) An oscillating head boundary was considered and not a line source representing well pumping. (2) The medium was taken as inclusion-type heterogeneity rather than random blocks considered here. (3) For realistic parameters, theory showed a small increase in K_{eq} , which could be on the same order of magnitude as numerical errors.

The results of this work are important for understanding the basic process of periodic groundwater flow. These processes arise not only considering oscillatory pumping tests, but also in a variety of other applications involving natural periodic aquifer variations, such as seasonal recharge or tidal impact on coastal aquifers. The equivalent conductivity is typically the first aquifer property to be estimated and understanding frequency dependence has both fundamental and practical significance. The current results indicate that despite the well documented physical phenomenon, field cases may actually present only with small K_{eq} variations with frequency and this may be due to measurement or modeling errors, rather than a physical mechanism discussed in the literature. A similar conclusion was mentioned in the previous literature [30], where it was stated that for most realistic parameters, the quasi-steady approximation (in which there is no frequency dependence of K_{eq}) is applicable. The main limitation of this work is that only two aquifer models were considered in the analysis, both with random lognormally distributed K . To reach a more definitive conclusion, future studies can test many cases with different types of heterogeneity. An additional limitation of the work is the discrepancy between the boundary condition used in the numerical (zero head at the vertical boundaries) and analytical (zero head at infinity for the horizontal direction) models, although this was accounted for in the results.

7. Summary and Conclusions

This work implemented a workflow for estimating the equivalent hydraulic conductivity of a heterogeneous aquifer from oscillatory pumping test head data. The method allows for multi-frequency pumping data to be analyzed and calculates K_{eq} for each frequency separately. The main goal of this work was to investigate the frequency dependence of K_{eq} in view of previous research, which was not conclusive on the significance and underlying cause of this phenomenon.

First, numerical simulations of the homogeneous aquifer problem were conducted for validation. Sufficient accuracy (less than 5%) of the numerical solution was found for a wide range of parameters. The limitations in terms of numerical error were investigated. It was found that for low and high frequencies, there is an increase in model error. For low frequencies, the error was found to be due to the zero head boundary condition in the numerical model (the analytical model assumes an infinite aquifer in the horizontal direction). For high frequencies, the error was associated with the exponentially decaying head which has large errors (in terms of percent of the measured head) when values are small. Next, two cases of heterogeneous aquifers were simulated and the output was used as synthetic head data for the K_{eq} estimation method. The first case of small K correlation length showed hardly any changes in K_{eq} (only about 6%) for a wide range of dimensionless frequency values. Values of K_{eq} increased for large and small frequencies as a result of numerical error. The second case of a larger K correlation length also showed minor variations of K_{eq} , yet slightly more than in Case 1 (about 15%). Variations were shown not to be related to the number of data points used in the method. However, the

variations were not a consistent increase with frequency as found in previous theoretical investigations, rather they consist of both decrease and increase. It was therefore suggested that the variations are due to numerical error and not a physical phenomenon.

Overall, this study did not find significant variations of K_{eq} with changing dimensionless frequency. The results of this work are important for practitioners conducting oscillatory pumping field tests. They indicate that the K_{eq} results should not change significantly with frequency and changes observed can be attributed to other measurement or method errors.

Author Contributions: Conceptualization, A.R.; Methodology, A.R.; Software, D.G.; Validation, D.G.; Investigation, D.G.; Writing—original draft, A.R. and D.G.; Writing—review & editing, A.R.; Supervision, A.R.; Project administration, A.R.; Funding acquisition, A.R. All authors have read and agreed to the published version of the manuscript.

Funding: This research received no external funding.

Data Availability Statement: Not applicable.

Conflicts of Interest: The authors declare no conflict of interest.

References

1. Kelly, B.F.; Timms, W.; Andersen, M.; McCallum, A.; Blakers, R.; Smith, R.; Rau, G.; Badenhop, A.; Ludowici, K.; Acworth, R. Aquifer heterogeneity and response time: The challenge for groundwater management. *Crop Pasture Sci.* **2013**, *64*, 1141–1154. [\[CrossRef\]](#)
2. Guo, Z.; Ma, R.; Zhang, Y.; Zheng, C. Contaminant transport in heterogeneous aquifers: A critical review of mechanisms and numerical methods of non-Fickian dispersion. *Sci. China Earth Sci.* **2021**, *64*, 1224–1241. [\[CrossRef\]](#)
3. Rasheed, Z.; Raza, A.; Gholami, R.; Rabiee, M.; Ismail, A.; Rasouli, V. A numerical study to assess the effect of heterogeneity on CO₂ storage potential of saline aquifers. *Energy Geosci.* **2020**, *1*, 20–27. [\[CrossRef\]](#)
4. Rudnik, G.; Rabinovich, A.; Siebner, H.; Katz, Y.; Kurtzman, D. Exploring Predictive Uncertainty at a Double-Source Managed Aquifer Recharge Site via Stochastic Modeling. *Water Resour. Res.* **2022**, *58*, e2021WR031241. [\[CrossRef\]](#)
5. Ferris, J.G. *Cyclic Fluctuations of Water Level as a Basis for Determining Aquifer Transmissibility*; Technical Report; US Geological Survey: Reston, VA, USA, 1952.
6. Johnson, C.R.; Greenkorn, R.; Woods, E. Pulse-testing: A new method for describing reservoir flow properties between wells. *J. Pet. Technol.* **1966**, *18*, 1–599. [\[CrossRef\]](#)
7. Kuo, C. Determination of reservoir properties from sinusoidal and multirate flow tests in one or more wells. *Soc. Pet. Eng. J.* **1972**, *12*, 499–507. [\[CrossRef\]](#)
8. Black, J.; Kipp, K. Determination of hydrogeological parameters using sinusoidal pressure tests: A theoretical appraisal. *Water Resour. Res.* **1981**, *17*, 686–692. [\[CrossRef\]](#)
9. Rasmussen, T.C.; Haborak, K.G.; Young, M.H. Estimating aquifer hydraulic properties using sinusoidal pumping at the Savannah River Site, South Carolina, USA. *Hydrogeol. J.* **2003**, *11*, 466–482. [\[CrossRef\]](#)
10. Dagan, G.; Rabinovich, A. Oscillatory pumping wells in phreatic, compressible, and homogeneous aquifers. *Water Resour. Res.* **2014**, *50*, 7058–7066. [\[CrossRef\]](#)
11. Cardiff, M.; Barrash, W. Analytical and Semi-Analytical Tools for the Design of Oscillatory Pumping Tests. *Groundwater* **2014**, *53*, 896–907. [\[CrossRef\]](#)
12. Song, I.; Renner, J. Analysis of oscillatory fluid flow through rock samples. *Geophys. J. Int.* **2007**, *170*, 195–204. [\[CrossRef\]](#)
13. Zhou, Y.; Lim, D.; Cupola, F.; Cardiff, M. Aquifer imaging with pressure waves—Evaluation of low-impact characterization through sandbox experiments. *Water Resour. Res.* **2016**, *52*, 2141–2156. [\[CrossRef\]](#)
14. Renner, J.; Messar, M. Periodic pumping tests. *Geophys. J. Int.* **2006**, *167*, 479–493. [\[CrossRef\]](#)
15. Guiltinan, E.; Becker, M.W. Measuring well hydraulic connectivity in fractured bedrock using periodic slug tests. *J. Hydrol.* **2015**, *521*, 100–107. [\[CrossRef\]](#)
16. Rabinovich, A.; Barrash, W.; Cardiff, M.; Hochstetler, D.L.; Bakhos, T.; Dagan, G.; Kitanidis, P.K. Frequency dependent hydraulic properties estimated from oscillatory pumping tests in an unconfined aquifer. *J. Hydrol.* **2015**, *531*, 2–16. [\[CrossRef\]](#)
17. Cheng, Y.; Renner, J. Exploratory use of periodic pumping tests for hydraulic characterization of faults. *Geophys. J. Int.* **2018**, *212*, 543–565. [\[CrossRef\]](#)
18. Marco, D.; Andrea, Z.; Fausto, C. Oscillatory pumping test to estimate aquifer hydraulic parameters in a Bayesian geostatistical framework. *Math. Geosci.* **2018**, *50*, 169–186. [\[CrossRef\]](#)
19. Fischer, P.; Jardani, A.; Jourde, H.; Cardiff, M.; Wang, X.; Chedeville, S.; Lecoq, N. Harmonic pumping tomography applied to image the hydraulic properties and interpret the connectivity of a karstic and fractured aquifer (Lez aquifer, France). *Adv. Water Resour.* **2018**, *119*, 227–244. [\[CrossRef\]](#)

20. Cardiff, M.; Zhou, Y.; Barrash, W.; Kitanidis, P.K. Aquifer imaging with oscillatory hydraulic tomography: Application at the field scale. *Groundwater* **2020**, *58*, 710–722. [[CrossRef](#)] [[PubMed](#)]
21. Bakhos, T.; Cardiff, M.; Barrash, W.; Kitanidis, P.K. Data processing for oscillatory pumping tests. *J. Hydrol.* **2014**, *511*, 310–319. [[CrossRef](#)]
22. Cheng, K.B.; Rabinovich, A.; Dagan, G. Stochastic modeling of oscillatory pumping in heterogeneous aquifers with application to Boise aquifer test. *J. Hydrol.* **2019**, *569*, 278–290. [[CrossRef](#)]
23. Cardiff, M.; Bakhos, T.; Kitanidis, P.; Barrash, W. Aquifer heterogeneity characterization with oscillatory pumping: Sensitivity analysis and imaging potential. *Water Resour. Res.* **2013**, *49*, 5395–5410. [[CrossRef](#)]
24. Fokker, P.A.; Renner, J.; Verga, F. Numerical modeling of periodic pumping tests in wells penetrating a heterogeneous aquifer. *Am. J. Environ. Sci.* **2013**, *9*, 1–13. [[CrossRef](#)]
25. Ahn, S.; Horne, R.N. Estimating permeability distributions from pressure pulse testing. In Proceedings of the SPE Annual Technical Conference and Exhibition, Society of Petroleum Engineers, Richardson, TX, USA, 6–8 October 2010.
26. Fokker, P.A.; Renner, J.; Verga, F. Applications of harmonic pulse testing to field cases. In Proceedings of the SPE Europec/EAGE Annual Conference, Society of Petroleum Engineers, Copenhagen, Denmark, 4–8 June 2012.
27. Fokker, P.A.; Borello, E.S.; Serazio, C.; Verga, F. Estimating reservoir heterogeneities from pulse testing. *J. Pet. Sci. Eng.* **2012**, *86*, 15–26. [[CrossRef](#)]
28. Patterson, J.R.; Cardiff, M. Aquifer Characterization and Uncertainty in Multi-Frequency Oscillatory Flow Tests: Approach and Insights. *Groundwater* **2021**, *60*, 180–191. [[CrossRef](#)] [[PubMed](#)]
29. Rabinovich, A.; Dagan, G.; Miloh, T. Dynamic effective properties of heterogeneous geological formations with spherical inclusions under periodic time variations. *Geophys. Res. Lett.* **2013**, *40*, 1345–1350. [[CrossRef](#)]
30. Rabinovich, A.; Dagan, G.; Miloh, T. Effective conductivity of heterogeneous aquifers in unsteady periodic flow. *Adv. Water Resour.* **2013**, *62*, 317–326. [[CrossRef](#)]
31. Cheng, K.B.; Dagan, G.; Barrash, W.; Cardiff, M.; Rabinovich, A. Statistical analysis of aquifer hydraulic properties by a continuous pumping tomography test: Application to the Boise Hydrogeophysical Research Site. *Water Resour. Res.* **2022**, *58*, e2022WR032464. [[CrossRef](#)]
32. Dagan, G. *Flow and Transport in Porous Formations*; Springer: Berlin/Heidelberg, Germany, 1989.
33. Brigham, E.O. *The Fast Fourier Transform and Its Applications*; Prentice-Hall, Inc.: Hoboken, NJ, USA, 1988.
34. Clement, T.; Jones, N. *RT3D Tutorials for GMS Users*; Technical Report; Pacific Northwest National Laboratory (PNNL): Richland, WA, USA, 1998.
35. Harbaugh, A.W.; Banta, E.R.; Hill, M.C.; McDonald, M.G. Modflow-2000. In *The US Geological Survey Modular Ground-Water Model-User Guide to Modularization Concepts and the Ground-Water Flow Process*; US Geological Survey: Reston, VA, USA, 2000.
36. Remy, N.; Boucher, A.; Wu, J.B. *Applied Geostatistics with SGeMS: A User's Guide*; Cambridge University Press: Cambridge, UK, 2009.
37. Pyrcz, M.; Deutsch, C. *Geostatistical Reservoir Modeling*; Oxford University Press: Oxford, UK, 2014.
38. Rehfeldt, K.R.; Boggs, J.M.; Gelhar, L.W. Field study of dispersion in a heterogeneous aquifer: 3. Geostatistical analysis of hydraulic conductivity. *Water Resour. Res.* **1992**, *28*, 3309–3324. [[CrossRef](#)]
39. Meerschaert, M.M.; Dogan, M.; Van Dam, R.L.; Hyndman, D.W.; Benson, D.A. Hydraulic conductivity fields: Gaussian or not? *Water Resour. Res.* **2013**, *49*, 4730–4737. [[CrossRef](#)]
40. Dagan, G. Higher-order correction of effective permeability of heterogeneous isotropic formations of lognormal conductivity distribution. *Transp. Porous Media* **1993**, *12*, 279–290. [[CrossRef](#)]

Disclaimer/Publisher's Note: The statements, opinions and data contained in all publications are solely those of the individual author(s) and contributor(s) and not of MDPI and/or the editor(s). MDPI and/or the editor(s) disclaim responsibility for any injury to people or property resulting from any ideas, methods, instructions or products referred to in the content.

